BioSystems 201 (2021) 104331

Contents lists available at ScienceDirect

BioSystems

journal homepage: http://www.elsevier.com/locate/biosystems

Cell and extracellular matrix growth theory and its implications for tumorigenesis

T.J. Sauer [a], E. Samei [a], A. Bejan [b,*]

[a] Duke University Medical School, Department of Radiology, Carl E. Ravin Advanced Imaging Laboratories, Durham, NC, 27705, USA
[b] Duke University, Department of Mechanical Engineering and Materials Science, Durham, NC, 27708-0300, USA

ARTICLE INFO

Keywords:
Cancer
Growth
Cluster
Step change
Transitions
Extracellular matrix (ECM)
Evolution
Constructal

ABSTRACT

Cells associated with an abnormal (cancerous) growth exchange flows, morph freely and grow hand-in-glove with their immediate environment, the extracellular matrix (ECM). The cell structure experiences two mass flows in counterflow. Flowing into the structure are nutrients and flowing out is refuse from the metabolically active biomass within. The physical effect of the evolution of the cell and extracellular structure is more flow and mixing in that space, that is, more mixing than in the absence of a biological growth in that space.

The objective of the present theory is to predict the increase in the size of the cell cluster as a function of its structure, and also to predict the critical cluster sizes that mark the transitions from one distinct cluster configuration to the next. This amounts to predicting the timing and the main features of the transitions from single cell to clusters with two, four, eight and more cells, including larger clusters with cells organized on its outer surface. The predicted evolution of the size and configuration of the cell cluster is validated successfully by comparison with measurements from several independent studies of cancerous and non-cancerous growth patterns.

1. Introduction

Animal design is an established and expanding field in biology and, more recently, in physics and the evolution of technology. Animal design is known by features, rules and 'efficiency' tendencies that are well documented in reference books (Schmidt-Nielsen, 1984; Wainwright et al., 1982; Charles and Bejan, 2009; Vogel, 1988; Weibel, 2000; Ahlborn, 2006; Zamir, 2000; Turner, 2009; Bejan and Lorente, 2011a) and is reviewed regularly (Hoppeler and Weibel, 2005; Reis, 2006; Bejan, 2020). Key examples are locomotion, respiration, blood circulation and vascularization, organism lifetime, mechanical strength, and the effect of body size on all observed features. Most of these advances are descriptive. They have been recorded as measurements, correlations, allometric rules and ad-hoc models that allow future scientists to calculate and reproduce (without repeating measurements) the physical features on which the models were based. Notable among these are models that utilize these descriptive advances (i.e., biophysical parameters) to inform their work such that they may be used in simulation studies of complex systems (Ghaffarizadeh et al., 2018; Hoehme and Drasdo, 2010; Van Liedekerke et al., 2020).

There are also advances of theoretical origin, which are predictive. Theoretical advances are the main features of animal biomechanics (static and dynamic) that are predicted from physics (mechanics) and now constitute textbook material in most universities (Schmidt-Nielsen, 1984; Wainwright et al., 1982; Charles and Bejan, 2009; Vogel, 1988; Weibel, 2000; Ahlborn, 2006; Zamir, 2000; Turner, 2009; Bejan and Lorente, 2011a; Hoppeler and Weibel, 2005; Reis, 2006; Bejan, 2020). More recently, theoretical steps are being made based on the view that the evolution (i.e., changes in flow configuration) is a distinct physics phenomenon governed by a self-standing law of physics (the constructal law). Examples are the complete architecture of lungs (Reis et al., 2004) and liver (Lorente et al., 2020), vegetation (Bejan et al., 2008), corals (Miguel, 2006), locomotion in all media (Bejan and Marden, 2006), social organization (Bejan et al., 2018), athletics (3), and the lifetime and life travel of everything that flows, moves and rolls, animate and inanimate (Bejan, 2012).

The new concept introduced by theory is that evolution belongs in physics, and that the flow system that evolves (animal, river basin, city) is not contemplated in isolation. This is a key feature necessary to describe fully the interaction of an abnormal biological growth with its local environment. Every system flows, morphs with freedom, grows and survives hand-in-glove with its immediate environment, which is its

* Corresponding author.
E-mail address: abejan@duke.edu (A. Bejan).

https://doi.org/10.1016/j.biosystems.2020.104331
Received 30 October 2020; Received in revised form 16 December 2020; Accepted 16 December 2020

'niche'. The environment is also a flow system that morphs freely and evolves.

In this paper, we focus on the system of cells associated with growth and self-organization. The environment of this system is the extracellular network supporting the cells. The system and its niche can be considered as one flow system, which has the freedom and time to change, and the space that enables the system to morph toward progressively greater flow access. Cells and the extracellular matrix (ECM) that facilitates the growth are a prime example of this kind (Hynes and Yamada, 2012; Ohki and Miyata, 2018; Keeley and Mecham, 2013). The unified structure is a flow system comprised of individual cells and their immediate environment. The ECM is the tissue network that gives a cluster of cells its structure and mechanical strength (Hynes and Yamada, 2012; Keeley and Mecham, 2013). Composed of various collagens with specialized functions, the ECM facilitates growth by acting as a 'scaffolding' to support new cells. The ECM also regulates cell migration through modifications to the local microenvironment.

The evolution of cell–ECM systems and their microenvironments can be analyzed through numerical simulations, which utilize biophysical parameters (e.g., cell mobility, cell–cell adhesion, cell size, etc.) (Ghaffarizadeh et al., 2018; Macklin et al., 2009) relevant to the phenomena of study and can be used to study particular biological effects on the growing system with independently operable parameters (Hoehme and Drasdo, 2010; Van Liedekerke et al., 2020; Wolkenhauer et al., 2014; Van Liedekerke et al., 2019). In the present work, however, we do not consider the results of any simulations, and our system has comparatively few biophysical parameters.

The cell structure experiences two mass flows in counterflow. Flowing into the structure are nutrients of flow rate $\dot{m}_{\text{in}}$ $[kg/s]$. Flowing out of the structure is refuse from the metabolically active biomass within; the discharge flow rate $\dot{m}_{\text{out}}$ $[kg/s]$ as shown in Fig. 1.

According to the constructal law, flow architectures that have freedom to morph will evolve naturally in order to provide greater access to the currents that flow. In the system–environment assembly the currents are $\dot{m}_{\text{in}}$ and $\dot{m}_{\text{out}}$. The physical effect of the evolution of the cell–extracellular structure is more flow and mixing in that space, i.e., more mixing than in the absence of a biological growth in that space. The constructal law calls for more and easier flow of nutrients and refuse, which governs both the morphological evolution of the flow structure as well as the evolution of nutrient transport complexity.

2. Methods

2.1. Model

What happens to the cell system over time is well-known empirically (Brekken and Stupack, 2017; Miner, 2005). Here we postulate the theoretical principles of this change over time. Fig. 2 illustrates the main features of this change process, which occurs both externally as the system size increases, and internally as the system structure changes stepwise and becomes more complex. In Fig. 2 the system is shown as a sphere; however, other single-scale models could be used (cube, tetrahedron, cylinder with height comparable to diameter, etc.). The key dimension of the system is the length scale D, or alternatively the surface area of scale D^2, and the volume of scale D^3— dimensions that translate proportionally to any three-dimensional primer that may be used in the model. This single dimension represents the size of the flow system.

Growth means that D will increase over time under conditions compatible with life. But how should the configuration of the system change over time? That is, what changes must happen in the complexity of nutrient transport in order to facilitate flow, growth and survival?

The time evolution of the system is shown in Fig. 3 as a sequence of three periods of growth. One period is the time interval when the internal structure does not change. From period to period, however, the structure changes stepwise. The three periods are distinct and defined by their internal structure:

1. Single cell, D_1.
2. Multicellular body, D_2, as a cluster of n cells of size D_1.
3. Vascular multicellular body D_3 requiring blood vessels of length scale D_3.

The objectives of the following theory are to predict the above scenario of how the body size $D(t)$ increases, and to predict the 'critical' sizes ($D_{1,2,3}$) that mark the transitions from one flow configuration to the next. This amounts to predicting the main features shown in Fig. 3 by accounting for the time arrow of evolution in all flow architectures that are free to morph.

2.2. Single cell

The single cell begins to grow in size at the time $t = 0$. The cell body has one length scale, $D(t)$. The cell grows because substances flow into it, being driven by concentration differences. When D is small enough, the flow is by diffusion. We account for concentration differences between the ECM and the cell with one order of magnitude, ΔC $[\text{kg/m}^3]$. The mass flow rate into the cell scales as

$$\dot{m} \sim A\alpha\frac{\Delta C}{\delta} \tag{1}$$

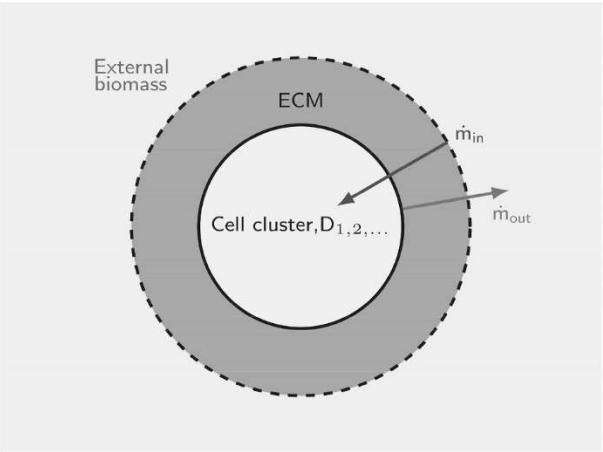

Fig. 1. The extracellular matrix (ECM) is shown with an embedded cluster of cells and their corresponding mass flows: $\dot{m}_{\text{in}}$ and $\dot{m}_{\text{out}}$, respectively.

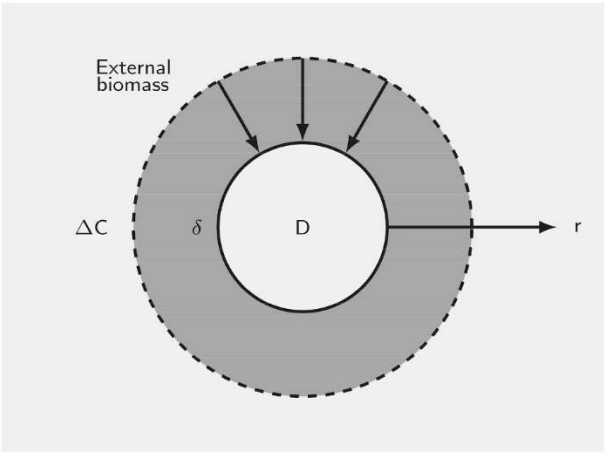

Fig. 2. Coordinate system for radial mass diffusion: the concentration gradient (ΔC), the boundary layer (δ), cell cluster size (D), direction of growth (r), and biomass external to the cell cluster are shown.

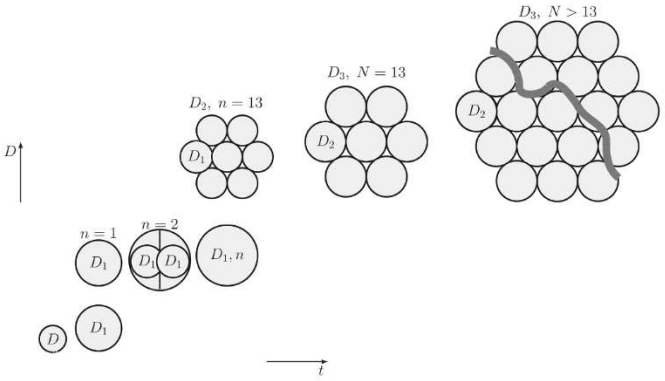

Fig. 3. Stepwise changes in diffusive flow architecture as the size of the cell cluster grows. D grows to maturity by diffusion to size D_1, which bifurcates into $n = 2$ cells of size D_1. The following transition shows a cluster of size D_2, consisting of one unit of $n = 13$ hexagonally-close-packed cells of size D_1. The subsequent transition shows a cluster of size D_3, consisting of $N = 13$ cell clusters of size D_2. The final transition indicates the need for vascularization beyond a critical size.

where $A \sim D^2$ is the scale of the surface area of the cell, and δ is the thickness of the diffusion layer that coats the cell (Fig. 2). The scale of δ follows from the diffusion equation written for the direction r away from the cell surface

$$\frac{dC}{dt} = \alpha \frac{d^2C}{dr^2} \tag{2}$$

where α [m^2 /s] is the mass diffusivity of the species C that diffuses through the ECM. Note that the origin of the r frame is attached to the cell surface (Fig. 2). As the cell grows, the r frame moves outward into the surroundings, and in turn the surroundings flow relative to the r frame inward with the speed

$$v \sim \frac{dD}{dt}. \tag{3}$$

Combining equations (2) and (3), and expressing the resulting equation in scale-analysis terms (namely, $r \sim D$ and $v \sim \alpha / D$), in place of equation (2) we obtain

$$\frac{D}{t}\frac{\Delta C}{D} \sim \alpha \frac{\Delta C}{\delta^2} \tag{4}$$

which yields

$$\delta \sim (\alpha t)^{1/2} \tag{5}$$

and, from equation (1),

$$\dot{m} \sim D^2 \alpha \frac{\Delta C}{(\alpha t)^{1/2}}. \tag{6}$$

The mass flow rate $\dot{m}$ is the scale of the rate of mass accumulation inside the cell,

$$\dot{m} \sim \frac{d}{dt}\left(CD^3\right) \tag{7}$$

where C [kg /m^3] is the density of the C species inside the cell volume. Eliminating $\dot{m}$ between equations (6) and (7) we obtain, in scaling terms,

$$D^2 \alpha \frac{\Delta C}{(\alpha t)^{1/2}} \sim \frac{CD^3}{t} \tag{8}$$

which yields

$$D \sim (\alpha t)^{1/2} \tag{9}$$

and, from equation (6),

$$\dot{m} \sim \alpha \Delta C (\alpha t)^{1/2}. \tag{10}$$

The conclusion of the above derivation is that δ is of the same order as D, and both dimensions grow as $(\alpha t)^{1/2}$. The bigger the cell, the bigger the external ECM necessary to accommodate it. The total mass flow rate, or the rate of cell growth, also grows as $t^{1/2}$. Because of the $t^{1/2}$ dependence, the total mass flow rate increases fastest in the beginning, and more slowly as time passes, as shown in Fig. 4.

In the following sections, the cell cycles of each of the individual cells in the cluster are assumed to be asynchronous. The primary difference between synchronous and asynchronous cell cycles is this: synchronous growth curves consist of compounded $\sqrt{\alpha t}$ curves (i.e., $D \propto \sqrt{\alpha t}$ between cell doublings, in light of equation (9)) following a macroscopic trend (cf., Figs. 1 and 2, in (Kubitschek, 1962) for similar behavior in *E. coli*.), while asynchronous cell cycle growth curves follow the macroscopic trend.

2.3. Small cluster

Next, consider a cluster of n cells of equal size (D_1), packed tightly such that each cell accounts for a portion of the external surface of the cluster

$$A_\Sigma \sim nD_1^2. \tag{11}$$

Properties of the cluster are indicated by the subscript Σ. The cluster diameter D_Σ follows from the same analysis as for equation (9),

$$D_\Sigma \sim (\alpha t)^{1/2}. \tag{12}$$

The cluster volume,

$$V_\Sigma \sim D_\Sigma^3 \sim nD_1^3 \tag{13}$$

in combination with equation (12) yields the number of cells n as a function of time,

$$n \sim \frac{(\alpha t)^{3/2}}{D_1^3}. \tag{14}$$

The calculation of the mass flow rate begins with rewriting equation (1) for the cluster,

$$\dot{m}_\Sigma \sim A_\Sigma \alpha \frac{\Delta C}{\delta_\Sigma} \tag{15}$$

and then using $\delta_\Sigma \sim (\alpha t)^{1/2}$ and equations (11) and (14),

$$\dot{m}_\Sigma \sim \alpha \Delta C \frac{\alpha t}{D_1}. \tag{16}$$

Compared with equation (10), equation (16) shows that the growth rate increases stepwise toward a faster mechanism as the configuration changes abruptly from a single cell to a cluster of cells (Fig. 4).

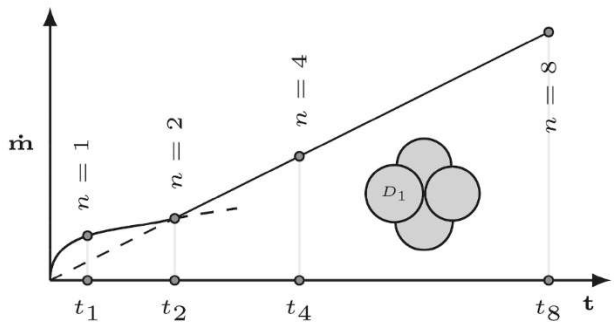

Fig. 4. Theoretical relationship between diffusion mass flow rate, time and cell cluster configuration. The bifurcation of the first cell is indicated from t_1 to t_2, and the bifurcation of both of those cells at t_4, and those cells again at t_8.

According to equation (9), if the single cell size D_1 is reached at the time t_1, then $D_1 \sim (\alpha t_1)^{1/2}$ and the transition marked by cell doubling in Fig. 4 occurs at time t_2,

$$2D_1 \sim (\alpha t_2)^{1/2} \tag{17}$$

which means that $t_2 \sim 4t_1$ if the total mass influx remains constant. Beyond the transition indicated as $n = 2$, tight clusters continue to emerge as each D_1 grows and then splits into two, and n increases from 2 to 4 and then 8. In view of equation (14), the times when $n = 4$ and $n = 8$ appear are ordered as follows

$$t_{0\to1} < t_{1\to2} < t_{2\to4} < \cdots. \tag{18}$$

These steps occur until the time when $n \sim 13$, at which point the central cell has no space to continue proliferating (i.e., cells here are assumed to be maximally contact-inhibited) as illustrated by the hexagonally–close-packed configuration in Fig. 5. This suggests that the presence of neighboring cells inhibits individual cell growth rates for the benefit of overall growth rate in accord with the constructal law.

These findings are supported by the correspondence between their predictions and experimental measurements gathered from images of small growing cell clusters (Kubitschek, 1962; Bean et al., 2006; Warburg et al., 1927; Mayneord, 1932a). Images from (Bean et al., 2006) were analyzed using a custom image segmentation algorithm to ensure standardized results; they also demonstrate the piecewise-growth behavior of cell clusters. A subset of the data acquired with this cell detection algorithm is shown in Fig. 6, and a representation of the results of the algorithm applied to a time series of cell images is shown in Fig. 9.

2.4. Large cluster

As the cluster continues to grow and its complexity increases, a time comes when the innermost cells cannot touch the outer surface A_Σ, and they can no longer proliferate by nutrient diffusion across the cluster surface. Beyond this time, the multiplying cells that thrive are those that touch A_Σ and exchange currents by diffusion with the ECM, as shown in Fig. 7.

The analysis of this new regime follows the same steps as in the preceding section [namely, $A_\Sigma \sim nD_1^2$, $D_\Sigma \sim (\alpha t)^{1/2}$] except that equation (13) is replaced by

$$D_\Sigma \sim A_\Sigma^{1/2} \sim n^{1/2} D_1, \tag{19}$$

where D_Σ is the cluster diameter. Equation (19) indicates that the number of cells in a small section of the periphery of the cluster ($n_{\text{peripheral}}$) grows linearly in time, $n_{\text{peripheral}} \sim \alpha t / D_1^2$, or that the volume of the cluster grows as t^3. The mass transfer rate of equation (15) in combination with $A_\Sigma \sim nD_1^2$ yields

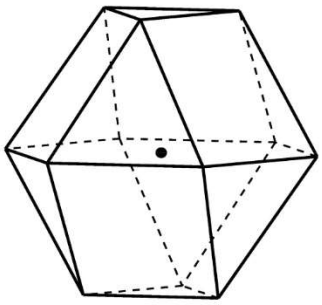

Fig. 5. Transition between small cluster configuration and large cluster configuration. Each vertex represents one cell of equal size with the central point representing the innermost cell, here assumed to be without space to reproduce. This is one configuration of the hexagonal close-packing pattern.

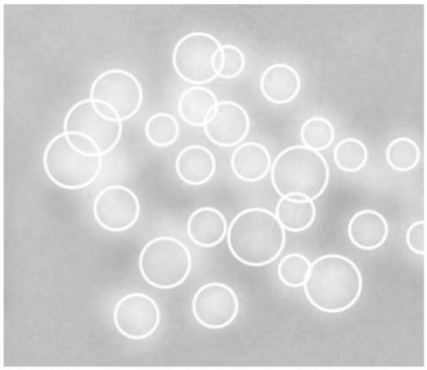

Fig. 6. The superimposed rings (white) show the output of the cell measuring algorithm, ensuring that cell sizes are objectively measured to the same standard at each time given a grayscale image of similar quality.

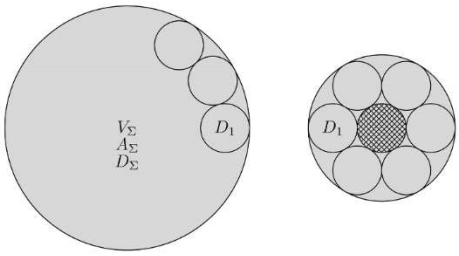

Fig. 7. Cell cluster of diameter, D_Σ, with cells on its surface, A_Σ, enclosed inside of a volume, V_Σ. Only the cells on the periphery have access to mass transfer with the ECM (left). The smallest possible configuration of this hexagonally–closed-packed cell cluster is shown on the right; the single shaded cell has no access to mass transfer.

$$\dot{m}_\Sigma \sim \alpha \Delta C (\alpha t)^{1/2}. \tag{20}$$

In equation (20), the time t is counted after the transition from tight packing (e.g., $n \approx 13$ in Fig. 4) to packing on the periphery (Fig. 7). The transition between the two regimes occurs when the cluster has become just large enough so that one cell (in the center of the cluster) does not have the ability to reproduce due to spatial constraints. That critical configuration is shown on the right side of Fig. 7,

$$D_\Sigma \sim 3D_1. \tag{21}$$

In view of equation (21), this transition occurs when $n \sim O(10)$.

Relative to the timeline of Fig. 4 (y-axis in units of $\dot{m}$, [kg/s]), the transition to Fig. 8 (y-axis in units of $D_{\text{effective}}\cdot[\mu m]$) occurs after cell doubling, $t \sim t_8$. Beyond this time point, which is between the first and second transitions in Fig. 10, the growth suddenly accelerates in the same manner as in the earliest stages of single cell growth.

From one regime to the next, the rate of growth increases stepwise. This is in accord with the evolutionary design tendency in other flow architectures in nature, such as snowflakes (Bejan et al., 2013) and dust clusters (Reis et al., 2006). The time sequence of Figs. 4–10 is in accord with observations. Another summary of the three scenarios (summarized in Table 1) is in terms of the growth of the number of cells and the diameter of the cluster. The growth is accelerated because of the stepwise changes in flow configuration.

2.5. Late large cluster

In the case of abundant nutrient influx to the cell cluster, the number of cells contained in the cluster grows in proportion with t^3, as shown in the Appendix. As the nutrient influx decreases because of limited availability, the number of cells present changes at a slower rate to

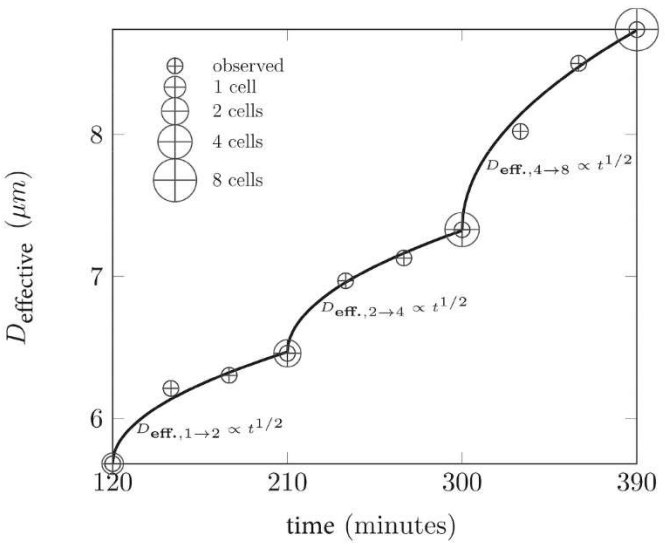

Fig. 8. Example yeast cell cluster growth: comparison between theoretical predictions (i.e., cluster diameter $\propto\sqrt{\alpha t}$ between cell doublings) and experimental measurements from Bean et al. (2006) of budding yeast cells, (see also Fig. 9).

accommodate this. If the number of cells that are able to continue reproducing decreases to a constant fraction of the cells on the surface (now additionally being nutrient-constrained rather than only space-constrained), the number of cells is proportional to t, and the diameter of the cell cluster is proportional to $t^{1/3}$.

2.6. Vascular cluster

The diffusion-limited growth of the cell cluster has a maximum size $D_{\max}$ (the last stage in Fig. 3), which is characterized by the diffusivity of oxygen in tissue α_{tis} and the characteristic time (t_{ch}) over which oxygen is delivered to the cell cluster and obeys the relation

$$D_{\max} \sim (\alpha_{\text{tis}} t_{\text{ch}})^{1/2}. \tag{22}$$

The diffusivity of oxygen in tissue of the type of interest is $\alpha_{\text{tis}} \sim 10^{-9}\,\text{m}^2/\text{s}$ (cf., Grote et al. (1977)), and the characteristic time is determined by the frequency of oxygen delivery and is of the order $t_{\text{ch}} \sim 1$ second for a heart rate of 60 beats per minute (Avram et al., 2019). Consequently, the maximum sustainable diffusion-limited growth size before internal cell death becomes inevitable is $O(10^2)\ \mu m$, in agreement with experimental data (Grote et al., 1977; Franko and Sutherland, 1979).

Beyond the size D_{max} the innermost cells require a new delivery mechanism for their nutrient supply, which is facilitated by the generation of a new vascular network.

3. Discussion

In this article, the combination of cell biology and constructal theory enabled quantitative predictions of fundamental characteristics of developing clusters of cells. The time-evolution of the size of cell clusters and the corresponding changes in nutrient transport complexity are predictable. In addition to the 'critical sizes', the analysis accounts for the changes in nutrient access complexity and geometry that dictate the evolution of the cell cluster into the next regime and configuration. This work reconciles the large-scale phenomenological models of cell proliferation (i.e., exponential and logistic growth models) with prior biological observations of cell clusters that disagreed in their description of small-scale and large-scale evolution. It provides insight into the scale of the individual cell as well as the multicellular cluster, rather than employing a purely microscopic (experimental) or macroscopic (model-based) approach. Furthermore, this work provides these insights without the need of computational implementations or simulations.

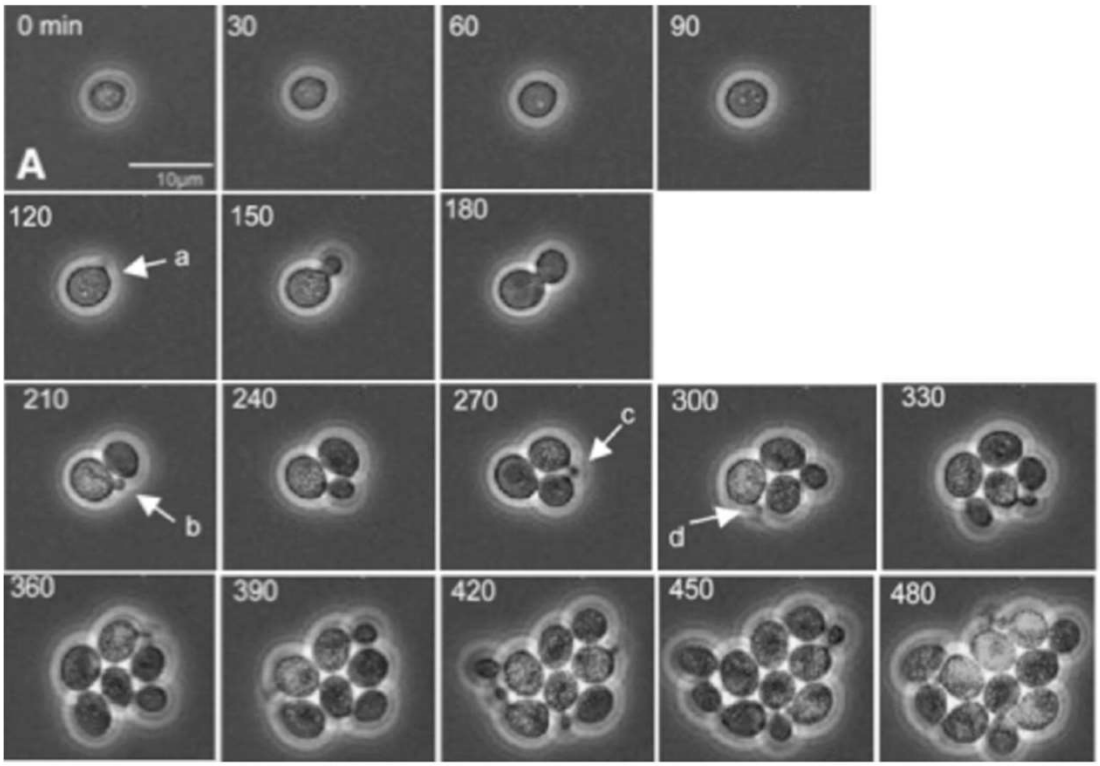

Fig. 9. Proliferating cells observed from Bean et al. (2006) at multiple time intervals in a controlled environment with labels $a, b, c, \ldots$ indicating the creation of a new cell.

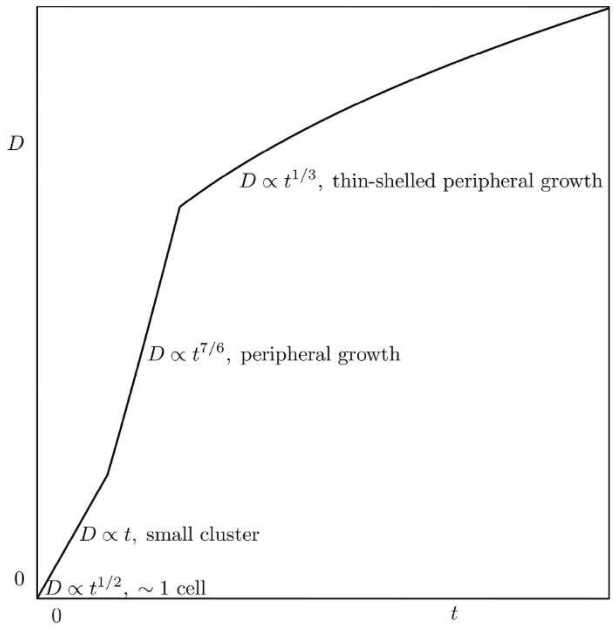

Fig. 10. Large-scale behavior of the cell cluster as it transitions from a small cluster exhibiting linear (diameter) growth up until only cells in a thin rim at the edge of the cell cluster can proliferate; to a large, nutrient-deprived cluster whose radius grows in proportion to $t^{1/3}$, in agreement with phenomenological logistic growth models. Note that this model does not acknowledge an "exponential growth" as present with a continuous growth rate proportional to the number of cells; however, the combination of the first 3 growth regimes qualitatively captures this behavior.

As shown by comparison of theory with experiment, the diffusion-based behavior of the growing cell has been validated repeatedly in the case of the growing cluster. Evidence of the synchronization of cell cycles—the timing and sequence of events required for a cell to produce offspring—and the resultant "resonant" effect support this theory. The resonant behavior occurs for temporally synchronized cell cycles and manifests as a compounded $\sqrt{at}$ curve. For asynchronous cell cycles, the compounded $\sqrt{at}$ structure is averaged such that the periodic behavior is not apparent. Both synchronous and asynchronous cell growth cycles can be described with this work.

The present theory assumes continuous growth by neglecting dormant periods between cell cycles. This assumption is appropriate in that it highlights the essential features of the growing cell cluster without introducing time-dependent biological details that would narrow the applicability or reduce the clarity of the work. The theory allows for insights into the early behavior of all biological domains of cell clusters, and specifically into the growth patterns and internal evolution of tumors.

The most natural application of this work is to the growth of localized, solid tumors (i.e., tumors not containing liquid or necrotic cores, and characterized by a limited cell mobility), as tumor cells most applicable to the present theory are undifferentiated or de-differentiate, unlike in healthy tissues (Gabbert et al., 1985; Magro et al., 2008; Yamada et al., 2019). The last row of Table 1 is particular to sufficiently large solid tumors: it addresses the case of surface-based cell proliferation, but under the special condition that (due to scarcity of nutrients, contact inhibition, or another cause) only a fixed number of cells can continue to proliferate per unit time. The limited proliferation results in the downturn of the characteristic S-curve (Turner, 2009) of growth, and it is indicative of macroscopic disease.

Beyond solid tumors, the present theory is relevant to non-solid cancers (e.g., leukemia, lymphoma, etc.). These cancers are frequently seen to have a faster initial growth rate compared to solid tumors (Shackney, 1970; Skipper et al., 1964; Wilcox, 1970; Rodriguez-Brenes et al., 2013). This can be attributed to the comparatively higher cell mobility, as the cells are not constrained to a solid tumor. The difference in mobility results in a characteristically prolonged period of high metabolic rate, indicative of minimal spatial constraints for proliferating cells. In the terminology of this work, this would indicate a longer period over which the "small cluster" dynamics describes the growth and metabolic rates. It should be noted, however, that there is no cluster to speak of in this case, only diffuse disease.

The current work is specific to growth and the subsequent overgrowth beyond available resources, which is an important feature in many cancers (Bouthelier and Lapunzina, 2005; Lapunzina, 2005; Waghorne et al., 1988; Colliniet al., 2012). If the theory is reformulated to apply to healthy (not abnormal) growth, we would not see an urgent necessity for vascular growth as in Section 2.6—the "invasion" of tumor cells would proceed more efficiently (i.e., with tree-shaped invasion (Cetkin et al., 2012; Bejan and Lorente, 2011b)).

The present work is specifically relevant to oncologic problems since many examples of cancers have been reported in the literature as being at least in part due to overgrowth; that is, growth that did not arrest or slow as expected with a decline in nutrients (Gabbert et al., 1985; Magro et al., 2008; Yamadaet al., 2019; Bouthelier and Lapunzina, 2005; Lapunzina, 2005; Waghorne et al., 1988; Colliniet al., 2012; Madsen et al., 2018).

In general, the present theory is applicable to aggressively growing cancers whose growth is constrained more by geometric limitations than biological (e.g., carcinoma in situ, which can be constrained to its original location by a basement membrane) (Lamm, 1992). Normal growth cannot proceed from the analysis presented in the paper, as this type of growth is naturally "parasitic". It enables its own growth at the expense of the tissue supporting it. This is sometimes due to genetic factors, and sometimes is a spontaneous change from benign tumor to malignant.

Because mechanisms of tumor complexity increase are revealed in the current theory, the theory leads to a quantitative understanding of the mechanics of nutrient transport and of the most effective approaches to corresponding treatments. The intuition that early tumor detection and treatment are most effective is supported. For example, when the tumor is small, the optimal time to apply a chemotherapeutic treatment is at the end of each (synchronous) cell cycle: the advantage in targeting this stage of growth is two-fold. The first advantage is that cells of the

Table 1
Scaling behavior of the number of cells, diameter of the cluster of cells and metabolic rate for single cells, small clusters of cells, and large clusters of cells in the diffusion-limited–growth regime. The expressions in the "Diameter" columns correspond directly to Fig. 10, where they are plotted.

	Number of cells (n)		Diameter of cell cluster (D)		Metabolic rate (m)
Single cell			$(at)^{1/2}$	$\sim$ 10 μm	$a\Delta C(at)^{1/2}$
Small cluster	$\left(\frac{at}{D_1^2}\right)^{3/2}$	$\sim 10^0 - 10^1$	$n^{1/3}(at)^{1/2}$	$\sim 10 - 30$ μm	$a\Delta C\frac{at}{D_1}$
Large cluster	$\frac{a}{D_1^2}t^3$	$\sim 10^1 - 10^3$	$(n^{2/3})^{1/3}(at)^{1/2}$	$\sim 10 - 100$ μm	$a\Delta C(at)^{1/2}$
Late large cluster	$(\text{const})t$	$\gtrsim 10^3$	$(\text{const})t^{1/3}$	$\gtrsim 100$ μm	$(\text{const})t^{1/3}$

tumor are still metabolically active but have not yet produced offspring, ensuring that all cells receive the required (lethal) dose of therapeutic agent–and that no cells are produced during the treatment, resulting in insufficient load to new cells. The second advantage is that the synchronization of cell cycles is far more robust when there are fewer cells, as they are better localized and subject to similar conditions. This synchronization (Nusse, 1981; Nusse, 1980; Breder et al., 1996) makes the timing of treatment more effective, and achieving cell-cycle synchrony has been previously acknowledged as a challenge for larger tumors (Zalatnai, 2005).

For the asynchronous cell cycles seen in larger tumors, treatment cannot be as effective as in the earliest synchronous stages, and it becomes significantly more difficult to eliminate all malignant cells. Conversely, for larger tumors it may be appropriate to target tumor cells not strictly as a function of malignant cell cycles, but as a function of the cell cycle of the surrounding healthy tissue. This approach can minimize the injury to healthy cells during therapy and aid in efforts to spare the load to radiosensitive organs (so as not to induce secondary cancers via treatment).

In sum, the biology of cell proliferation and the application of constructal growth physics has resulted in a theory that predicts the behavior of clusters of cells as they increase in size, number and complexity. This work provides a unifying perspective on the time-evolution of cell clusters on the smallest scales, as observed experimentally in biology, and the large-scale dynamics of proliferating cells as described in phenomenological models. The present theory does this with the simultaneous strengths of predicting behavior on the smallest and largest scales.

Declaration of competing interest

The authors declare that they have no known competing financial interests or personal relationships that could have appeared to influence the work reported in this paper.

Appendix

With reference to the discussion in section 6, we write V, R, β and $r^\star$ for the volume of cluster, radius of cluster, fraction of cells in the shell still proliferating *per unit time*, and the thickness of the rim of proliferating cells near the surface of the cluster (A.1).

Combining

$$\frac{dV}{dt} \propto \beta\left(r^3 - (r - r^\star)^3\right) \tag{A.1}$$

$$dV \propto r^2 dr \tag{A.2}$$

we obtain

$$\frac{dr}{dt} \propto \beta\left(r^\star - \frac{r^{\star 2}}{r} + \frac{r^{\star 3}}{3r^2}\right). \tag{A.3}$$

Rearranging (A.3) and applying scale analysis (A.2), we obtain

$$r\left(r^2 - \beta r^\star \Delta t r + \beta r^{\star 2}\Delta t\right) \sim \frac{\beta r^{\star 3}\Delta t}{3}. \tag{A.4}$$

If the cell cluster is in a nutrient-limited stage of growth, a constant number of cells will divide per unit time and is located in a thin shell at the surface of the cluster. If β is a constant of $O(r^\star)$ and $r^\star \ll r$, the r^3 term dominates the left-hand side of (A.4),

$$r^3 \sim \frac{\beta r^{\star 3}\Delta t}{3} \tag{A.5}$$

cf., (Bejan, 2013; Mayneord, 1932b).

References

Ahlborn, B.K., 2006. Zoological Physics: Quantitative Models of Body Design, Actions, and Physical Limitations of Animals. Springer Science & Business Media.

Avram, R., Tison, G.H., Aschbacher, K., Kuhar, P., Vittinghoff, E., Butzner, M., Runge, R., Wu, N., Pletcher, M.J., Marcus, G.M., Olgin, J., 2019. Real-world heart rate norms in the Health eHeart study. npj Digital Medicine 2 (1), 58. https://doi.org/10.1038/s41746-019-0134-9.

Bean, J.M., Siggia, E.D., Cross, F.R., 2006. Coherence and timing of cell cycle start examined at single-cell resolution. Mol. Cell 21 (1), 3–14. https://doi.org/10.1016/j.molcel.2005.10.035.

Bejan, A., 2012. Why the bigger live longer and travel farther: animals, vehicles, rivers and the winds. Sci. Rep. 2, 594. https://doi.org/10.1038/srep00594.

Bejan, A., 2013. Convection Heat Transfer, fourth ed. Wiley, Hoboken.

Bejan, A., 2020. Human evolution is biological & technological evolution. Biosystems 195, 104156.

Bejan, A., Lorente, S., 2011a. The constructal law origin of the logistics S curve. J. Appl. Phys. 110, 024901.

Bejan, A., Lorente, S., 2011b. The constructal law origin of the logistics S curve. J. Appl. Phys. 110, 024901.

Bejan, A., Marden, J.H., 2006. Unifying constructal theory for scale effects in running, swimming and flying. J. Exp. Biol. 209 (Pt 2), 238–248. https://doi.org/10.1242/jeb.01974.

Bejan, A., Lorente, S., Lee, J., 2008. Unifying constructal theory of tree roots, canopies and forests. J. Theor. Biol. 254 (3), 529–540. https://doi.org/10.1016/j.jtbi.2008.06.026.

Bejan, A., Lorente, S., Yilbas, B.S., Sahin, A.Z., 2013. Why solidification has an S-shaped history. Sci. Rep. 3, 1711. EP -.

Bejan, A., Gunes, U., Errera, M.R., Sahin, B., 2018. Social organization: the thermodynamic basis. Int. J. Energy Res. 42 (12), 3770–3779. https://doi.org/10.1002/er.4093.

Bouthelier, R.G., Lapunzina, P., 2005. Follow-up and risk of tumors in overgrowth syndromes. J. Pediatr. Endocrinol. Metab. 18 (Suppl. ment), 1227–1236.

Breder, J., Ruller, S., Ruller, E., Schlaak, M., vanderBosch, J., 1996. Induction of cell death by cytokines in cell cycle-synchronous tumor cell populations restricted to G (1) and G(2). Exp. Cell Res. 223 (2), 259–267. https://doi.org/10.1006/excr.1996.0080.

Brekken, R.A., Stupack, D., 2017. Extracellular Matrix in Tumor Biology. Springer.

Cetkin, E., Lorente, S., Bejan, A., 2012. The steepest S curve of spreading and collecting flows: discovering the invading tree, not assuming it. J. Appl. Phys. 111, 114903.

Charles, J.D., Bejan, A., 2009. The evolution of speed, size and shape in modern athletics. J. Exp. Biol. 212 (Pt 15), 2419–2425. https://doi.org/10.1242/jeb.031161.

Collini, P., et al., 2012. High-grade sarcomatous overgrowth in solitary fibrous tumors: a clinicopathologic study of 10 cases. Am. J. Surg. Pathol. 36, 1202–1215.

Franko, A.J., Sutherland, R.M., 1979. Oxygen diffusion distance and development of necrosis in multicell spheroids. Radiat. Res. 79 (3), 439–453. https://doi.org/10.2307/3575173.

Gabbert, H., Wagner, R., Moll, R., Gerharz, C.-D., 1985. Tumor dedifferentiation: an important step in tumor invasion. Clin. Exp. Metastasis 3, 257–279.
Ghaffarizadeh, A., Heiland, R., Friedman, S.H., Mumenthaler, S.M., Macklin, P., 2018. PhysiCell: an open source physics-based cell simulator for 3-D multicellular systems. PLoS Comput. Biol. 14 (2), e1005991 https://doi.org/10.1371/journal.pcbi.1005991.
Grote, J., Süsskind, R., Vaupel, P., 1977. Oxygen diffusivity in tumor tissue (DS-Carcinosarcoma) under temperature conditions within the range of 20–40°C. Pflügers Archiv 372 (1), 37–42. https://doi.org/10.1007/BF00582204.
Hoehme, S., Drasdo, D., 2010. A cell-based simulation software for multi-cellular systems. Bioinformatics 26 (20), 2641–2642. https://doi.org/10.1093/bioinformatics/btq437.
Hoppeler, H., Weibel, E.R., 2005. Scaling functions to body size: theories and facts. J. Exp. Biol. 208 (Pt 9), 1573–1574. https://doi.org/10.1242/jeb.01630.
Hynes, R.O., Yamada, K.M., 2012. Extracellular Matrix Biology. Cold Spring Harbor Laboratory Press.
Keeley, F.W., Mecham, R., 2013. Evolution of Extracellular Matrix. Springer Science & Business Media.
Kubitschek, H.E., 1962. Normal distribution of cell generation rate. Exp. Cell Res. 26 (3), 439–450. https://doi.org/10.1016/0014-4827(62)90150-7.
Lamm, D., 1992. Carcinoma in Situ, vol. 19. The Urologic Clinics of North America, pp. 499–508.
Lapunzina, P., 2005. Risk of tumorigenesis in overgrowth syndromes: a comprehensive review. In: American Journal of Medical Genetics Part C: Seminars in Medical Genetics, vol. 137. Wiley Online Library, pp. 53–71.
Lorente, S., Hautefeuille, M., Sanchez-Cedillo, A., 2020. The liver, a functionalizd vascular structure. Sci. Rep. 10, 16194. https://doi.org/10.1038/s41598-020-73208-8.
Macklin, P., McDougall, S., Anderson, A.R.A., Chaplain, M.A.J., Cristini, V., Lowengrub, J., 2009. Multiscale modelling and nonlinear simulation of vascular tumour growth. J. Math. Biol. 58 (4–5), 765–798. https://doi.org/10.1007/s00285-008-0216-9.
Madsen, R.R., Vanhaesebroeck, B., Semple, R.K., 2018. Cancer-associated PIK3CA mutations in overgrowth disorders. Trends Mol. Med. 24, 856–870.
Magro, G., Emmanuele, C., Lopes, M., Vallone, G., Greco, P., 2008. Solitary fibrous tumour of the kidney with sarcomatous overgrowth. Case report and review of the literature. Apmis 116, 1020–1025.
Mayneord, W.V., 1932a. On a law of growth of jensen's rat sarcoma. Am. J. Canc. 16 (4), 841–846. https://doi.org/10.1158/ajc.1932.841.
Mayneord, W.V., 1932b. On a law of growth of jensen's rat sarcoma. Am. J. Canc. 16, 841–846. https://doi.org/10.1158/ajc.1932.841.
Miguel, A.F., 2006. Constructal pattern formation in stony corals, bacterial colonies and plant roots under different hydrodynamics conditions. J. Theor. Biol. 242 (4), 954–961. https://doi.org/10.1016/j.jtbi.2006.05.010.
Miner, J.H., 2005. Extracellular Matrix in Development and Disease. Elsevier.
Nusse, M., 1980. Cell-cycle kinetics of synchronous and asynchronous tumor-cells invitro after irradiation with X-rays and alpha-particles during the cell-cycle - analysis of flow micro-fluorometric data. Radiat. Environ. Biophys. 17 (4), 296-296.
Nusse, M., 1981. Cell-cycle kinetics of irradiated synchronous and asynchronous tumor-cells with DNA distribution analysis and brdurd-hoechst 33258-technique. Cytometry 2 (2), 70–79. https://doi.org/10.1002/cyto.990020206.
Ohki, K., Miyata, H., 2018. Physical Principles of Biomembranes and Cells. Springer.
Reis, A.H., 2006. Constructal theory: from engineering to physics, and how flow systems develop shape and structure. Appl. Mech. Rev. 59 (1–6), 269–282. https://doi.org/10.1115/1.2204075.
Reis, A.H., Miguel, A.F., Aydin, M., 2004. Constructal theory of flow architecture of the lungs. Med. Phys. 31 (5), 1135–1140. https://doi.org/10.1118/1.1705443.
Reis, A.H., Miguel, A.F., Bejan, A., 2006. Constructal theory of particle agglomeration and design of air-cleaning devices. J. Phys. Appl. Phys. 39 (10), 2311–2318. https://doi.org/10.1088/0022-3727/39/10/046.
Rodriguez-Brenes, I.A., Komarova, N.L., Wodarz, D., 2013. Tumor growth dynamics: insights into evolutionary processes. Trends Ecol. Evol. 28 (10), 597–604. https://doi.org/10.1016/j.tree.2013.05.020.
Schmidt-Nielsen, K., 1984. Why Is Animal Size So Important? Cambridge University Press.
Shackney, S.E., 1970. A computer model for tumor growth and chemotherapy, and its application to L1210 leukemia treated with cytosine arabinoside (NSC-63878). Cancer Chemother. Rep. 54 (6), 399–429.
Skipper, H.E., Schabel Jr., F.M., Wilcox, W.S., 1964. Experimental evaluation of potential anticancer agents. Xiii. On the criteria and kinetics associated with "curability" of experimental leukemia. Cancer Chemother. Rep. 35, 1–111.
Turner, J.S., 2009. The Tinkerer's Accomplice. Harvard University Press.
Van Liedekerke, P., Neitsch, J., Johann, T., Alessandri, K., Nassoy, P., Drasdo, D., 2019. Quantitative cell-based model predicts mechanical stress response of growing tumor spheroids over various growth conditions and cell lines. PLoS Comput. Biol. 15 (3), e1006273 https://doi.org/10.1371/journal.pcbi.1006273.
Van Liedekerke, P., Neitsch, J., Johann, T., Warmt, E., Gonzalez-Valverde, I., Hoehme, S., Grosser, S., Kaes, J., Drasdo, D., 2020. A quantitative high-resolution computational mechanics cell model for growing and regenerating tissues. Biomech. Model. Mechanobiol. 19 (1), 189–220. https://doi.org/10.1007/s10237-019-01204-7.
Vogel, S., 1988. Life's Devices: the Physical World of Animals and Plants. Princeton University Press.
Waghorne, C., Thomas, M., Lagarde, A., Kerbel, R., Breitman, M., 1988. Genetic evidence for progressive selection and overgrowth of primary tumors by metastatic cell subpopulations. Canc. Res. 48, 6109–6114.
Wainwright, S.A., Biggs, W.D., Currey, J.D., 1982. Mechanical Design in Organisms. Princeton University Press.
Warburg, O., Wind, F., Negelein, E., 1927. The metabolism OF tumors IN the body. J. Gen. Physiol. 8 (6), 519–530.
Weibel, E.R., 2000. Symmorphosis: on Form and Function in Shaping Life. Harvard University Press.
Wilcox, W.S., 1970. The last surviving cancer cell: the chances of killing it. CA A Cancer J. Clin. 20 (3), 164–167. https://doi.org/10.3322/canjclin.20.3.164.
Wolkenhauer, O., Auffray, C., Brass, O., Clairambault, J., Deutsch, A., Drasdo, D., Gervasio, F., Preziosi, L., Maini, P., Marciniak-Czochra, A., Kossow, C., Kuepfer, L., Rateitschak, K., Ramis-Conde, I., Ribba, B., Schuppert, A., Smallwood, R., Stamatakos, G., Winter, F., Byrne, H., 2014. Enabling multiscale modeling in systems medicine. Genome Med. 6 (3), 21. https://doi.org/10.1186/gm538.
Yamada, Y., et al., 2019. Clinicopathological review of solitary fibrous tumors: dedifferentiation is a major cause of patient death. Virchows Arch. 475, 467–477.
Zalatnai, A., 2005. Potential role of cell cycle synchronizing agents in combination treatment modalities of malignant tumors. *In* Vivo 19 (1), 85–91.
Zamir, M., 2000. The Physics of Pulsatile Flow. Springer Science & Business Media.